Journal of Power Sources 195 (2010) 1416–1426

Contents lists available at ScienceDirect

Journal of Power Sources

journal homepage: www.elsevier.com/locate/jpowsour

The empirical validation of a model for simulating the thermal and electrical performance of fuel cell micro-cogeneration devices

Ian Beausoleil-Morrison*

Department of Mechanical & Aerospace Engineering, Carleton University, 1125 Colonel By Drive, 3135 Mackenzie Building, Ottawa, Ontario, Canada K1S 5B6

ARTICLE INFO

Article history:
Received 12 June 2009
Accepted 7 September 2009
Available online 11 September 2009

Keywords:
Fuel cell micro-cogeneration
Empirical validation

ABSTRACT

Fuel cell micro-cogeneration is a nascent technology that can potentially reduce the energy consumption and environmental impact associated with serving building electrical and thermal demands. Accurately assessing these potential benefits and optimizing the integration of micro-cogeneration within buildings requires simulation methods that enable the integrated modelling of fuel cell micro-cogeneration devices with the thermal and electrical performance of the host building and other plant components. Such a model has recently been developed and implemented into a number of building simulation programs as part of an International Energy Agency research project. To date, the model has been calibrated (tuned) for one particular prototype 2.8 kW_{AC} solid-oxide fuel cell (SOFC) micro-cogeneration device. The current paper examines the validity of this model by contrasting simulation predictions to measurements from the 2.8 kW_{AC} prototype device. Good agreement was found in the predictions of DC power production, the rate of fuel consumption, and energy conversion efficiencies. Although there was greater deviation between simulation predictions and measurements in the predictions of useful thermal output, acceptable agreement was found within the uncertainty of the model and the measurements. It is concluded that the form of the mathematical model can accurately represents the performance of SOFC micro-cogeneration devices and that detailed performance assessments can now be performed with the calibrated model to examine the applicability of the 2.8 kW_{AC} prototype device for supplying building electrical and thermal energy requirements.

1. Introduction

Fuel cell micro-cogeneration devices concurrently produce electricity and heat from a single fuel source at a scale that is suitable for use in single-family houses ($< 15\ kW_e$). These emerging technologies offer a number of potential benefits: reduced primary energy consumption, reduced greenhouse gas emissions, reduced electrical transmission and distribution losses, and alleviation of electrical grid congestion during peak periods. Numerous companies are actively developing fuel cell micro-cogeneration devices and introducing these to market [1,2].

Fuel cell micro-cogeneration devices have only modest fuel-to-electrical conversion efficiencies. Several researchers have measured the performance of natural-gas-fired prototype devices based upon proton exchange membrane (PEMFC) and solid-oxide fuel cells (SOFC) [3–13]. They have found efficiencies to be in the range of 10–40% in terms of the net alternating current (AC) electrical output relative to the source fuel's lower heating value (LHV). Promising results have also been obtained with a developmental alkaline fuel cell (AFC) device [14].

Although these results are encouraging for early prototypes, these electrical efficiencies are relatively low compared to state-of-the-art natural-gas-fired central power generation: combined-cycle central power plants can achieve efficiencies in the order of 55% [15,16]. As such, if fuel cell micro-cogeneration is to compete with the best-available central power generation technologies, it is critical that the thermal output be well utilized. Potential uses of this thermal output include space heating, domestic hot water (DHW) heating, and space cooling (through a thermally activated cycle).

Therefore, in order to accurately assess the overall energy performance of fuel cell micro-cogeneration and to optimize integration and control strategies it is imperative that the coupling between the micro-cogeneration device, supporting components for transferring and converting the thermal output, the building, its occupants, and climate be considered in an integrated fashion. Such an integrated modelling approach could be used to explore answers to significant questions on the applicability and impact of the technology, such as

* Corresponding author. Tel.: +1 613 520 2600; fax: +1 613 520 5715.
E-mail address: Ian_Beausoleil-Morrison@carleton.ca.

0378-7753/$ – see front matter © 2009 Elsevier B.V. All rights reserved.
doi:10.1016/j.jpowsour.2009.09.013

- What are the net energy and greenhouse gas (GHG) impacts and the impact upon the central electrical grid?
- What combinations of building envelopes, occupancy patterns, and climate are favourable for micro-cogeneration?
- What are the optimal dispatch strategies: electric load following, thermal load following, economic dispatch, minimization of GHG emissions from the central electrical grid?
- How should the building's thermal plant (thermal storage, auxiliary heating, pumps, heat exchangers) be designed and controlled to maximally exploit the thermal output?
- What are the appropriate electrical generation and thermal storage capacities for single-family and multi-family housing?

These factors motivated the formation of Annex 42 of the International Energy Agency's Energy Conservation in Buildings and Community Systems Programme (IEA/ECBCS). This international collaborative project developed, validated, and implemented models of micro-cogeneration devices for whole-building simulation programs. The IEA/ECBCS Annex 42 mathematical model for simulating the performance of fuel cell micro-cogeneration systems [17,18] is a system-level quasi-steady-state model that considers the thermodynamic performance of all components that consume energy and produce thermal and electrical output. The model relies heavily upon empirical information that can be acquired from the testing of coherent systems or components and is designed for operation at a time resolution in the order of minutes.

This model has been calibrated (i.e. its input data established) to represent the performance of a 2.8 kW_{AC} SOFC micro-cogeneration device [19,13]. A series of 45 experiments were conducted on this device under varied and controlled boundary conditions. Measurements of the device's fuel and air consumption, power production, thermal output, etc., under these operating conditions were used to calibrate the various aspects of the model.

Sixteen additional experiments were performed with different combinations of boundary conditions. These experiments were disjunct from the 45 experiments whose data were used to calibrate the model (the *calibration experiments*). The current paper uses the data from these 16 *validation experiments* to examine the validity of the mathematical model (as described in [17,18]) and the accuracy of its calibration (as documented in [19,13]).

A brief review of pertinent aspects of the mathematical model is first provided, followed by a concise presentation of the model's calibration to represent the prototype SOFC micro-cogeneration device. The majority of the paper is dedicated to comparisons between simulations conducted with the calibrated model and measurements from the validation experiments.

2. Model description

The fuel cell micro-cogeneration model is based upon an energy balance approach. For reasons of extensibility and adaptability it discretizes the micro-cogeneration system's components into control volumes that produce electrical power, supply air, capture heat from the hot product gases, etc. Energy balances are formed and solved for each control volume on a time-step basis, this to accurately treat the interactions with the building, the occupants, and control systems. Each control volume is modelled in as rigorous a fashion as possible given the constraints of computational efficiency and the need to calibrate model inputs based upon the testing of coherent systems.

The discretization scheme is illustrated in Fig. 1. Each control volume is identified with italicized text and represented by dashed lines. Mass and heat flows are indicated with solid arrows. In this figure only the control volumes pertinent to the SOFC micro-cogeneration device considered in the current paper are illustrated for the sake of clarity. These include:

- The fuel cell power module (FCPM) which includes the reformer, stack, and afterburner. This control volume is supplied with streams of air and fuel and produces a stream of hot product gases resulting from the electrochemical and combustion reactions. The FCPM's net direct current (DC) power production exits the control volume. This control volume also transfers heat to the dilution air control volume and to the containing room.
- An exhaust-gas-to-water heat exchanger. This device transfer heat from the incoming hot product gases and transfers this energy to a water stream which is coupled to the building's heating plant, that is it produces the device's useful thermal output.
- A DC–AC power conditioning unit.
- A dilution air system with optional heat recovery ventilator as used in some systems to draw air through the cabinet to control skin losses to the containing room. This control volume is supplied with cool air and receives a heat transfer from the FCPM. The heated air exiting the dilution air control volume is mixed with the heat exchanger's cooled product gases to form the device's exhaust-gas stream.

The interested reader is referred to [18,17] for a complete representation of the model, which can be configured to represent both SOFC and PEMFC micro-cogeneration devices.

Relevant aspects of the model's treatment of the individual control volumes are presented in the following subsections.

2.1. Energy balances

The fuel cell's stack, reformer, and afterburner are represented by a control volume known as the fuel cell power module (FCPM). Its energy balance can be written in the following form,[1]

$$\dot{H}_{\text{fuel}} + \dot{H}_{\text{air}} = P_{\text{el}} + \dot{H}_{\text{FCPM-cg}} + q_{\text{skin-loss}} + q_{\text{FCPM-to-dilution}} \quad (1)$$

where $\dot{H}_{\text{fuel}}$ and $\dot{H}_{\text{air}}$ represent the enthalpy carried into the control volume by the fuel and by the air required to support electrochemical and combustion reactions, as well as the excess air. P_{el} is the net DC power production, that is the stack power less ohmic losses in cabling and the power draw of ancillaries such as the fan that supplies the air. $\dot{H}_{\text{FCPM-cg}}$ represents the enthalpy carried out of the control volume by the exiting gas stream composed of the products of the electrochemical and combustion reactions, the excess air, and the inert constituents of the fuel. The final two terms in Eq. (1) represent thermal losses: $q_{\text{skin-loss}}$ is the radiant and convective heat transfer to the containing room while $q_{\text{FCPM-to-dilution}}$ represents the heat transfer from the FCPM to the air stream which is drawn through the micro-cogeneration device's cabinet to comply with gas venting requirements of safety codes.

The thermal energy of the FCPM's hot exhaust gases (represented by the $\dot{H}_{\text{FCPM-cg}}$ term in Eq. (1)) is transferred through a heat exchanger to a water loop connected to the building's plant. This provides the micro-cogeneration device's useful thermal output (q_{HX}). The sensible component of this heat transfer is characterized with the log mean temperature difference (LMTD) method for counterflow heat exchangers while the latent term is characterized

[1] The structure of the model is generic in order to treat all fuel cell micro-cogeneration systems including PEMFC. Terms that are not relevant to the particular SOFC micro-cogeneration device treated in this paper are not shown here for the sake of clarity.

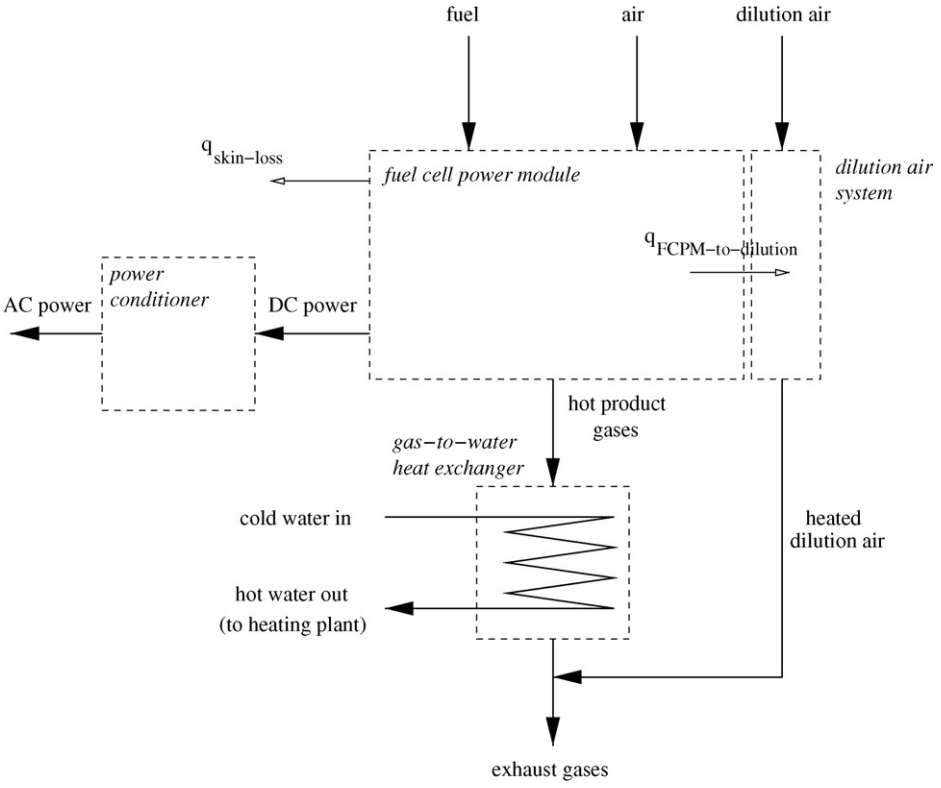

Fig. 1. Model discretization.

by estimating the rate of condensation. This is given by

$$\begin{aligned} q_{HX} &= q_{sensible} + q_{latent} \\ &= (UA)_{eff} \cdot \frac{(T_{FCPM\text{-}cg} - T_{w\text{-}out}) - (T_{g\text{-}out} - T_{w\text{-}in})}{\ln((T_{FCPM\text{-}cg} - T_{w\text{-}out})/(T_{g\text{-}out} - T_{w\text{-}in}))} \\ &\quad + \dot{N}_{H_2O\text{-}cond} \cdot \hat{h}_{fg} \end{aligned} \tag{2}$$

where $T_{FCPM\text{-}cg}$ is the temperature of the hot gases exiting the FCPM and entering the heat exchanger and $T_{g\text{-}out}$ is the temperature of the cooled gases exiting the heat exchanger. $T_{w\text{-}in}$ is the temperature of the cold water at the heat exchanger inlet and $T_{w\text{-}out}$ is the temperature of the warmed water exiting the heat exchanger. $(UA)_{eff}$ is the effective product of the heat transfer coefficient and area ($W\,K^{-1}$). $\dot{N}_{H_2O\text{-}cond}$ is the rate of condensation of water from the gas stream ($kmol\,s^{-1}$) and $\hat{h}_{fg}$ is the molar heat of vapourization of water ($J\,kmol^{-1}$).

A power conditioning system converts the FCPM's DC output to AC power to supply the building's electrical loads and perhaps to export power to the grid. A simple energy balance is used to represent the control volume for this device

$$P_{AC} = \eta_{PCU} \cdot P_{el} \tag{3}$$

where P_{AC} represents the micro-cogeneration device's AC power production and η_{PCU} is the DC–AC power conversion efficiency.

Eqs. (1)–(3) outline the methods used to characterize the energy balances for three of the model's control volumes. Similar techniques are employed for the remaining six control volumes.

2.2. Empirical coefficients

There is a great deal of interdependency between the energy balances representing each control volume as well as between the individual terms of the energy balances. For example, the net DC power production (appearing in Eqs. (1) and (3)) is related to the fuel consumption (and thus the $\dot{H}_{fuel}$ term of Eq. (1)) through the FCPM's electrical efficiency

$$\epsilon_{el} = \frac{P_{el}}{\dot{N}_{fuel} \cdot LHV_{fuel}} \tag{4}$$

where ϵ_{el} is the electrical efficiency and $\dot{N}_{fuel}$ is the molar flow rate of the fuel.

Many of the individual terms of the energy balances are empirical in nature and are evaluated on a time-step basis. For example, the FCPM's electrical efficiency required by Eq. (4) is given by,[2]

$$\epsilon_{el} = \epsilon_0 + \epsilon_1 \cdot P_{el} + \epsilon_2 \cdot P_{el}^2 \tag{5}$$

where ϵ_i are empirical coefficients.

Similarly, $(UA)_{eff}$ required in Eq. (2) is expressed as a parametric relation of the water ($\dot{N}_w$) and gas ($\dot{N}_g$) flow rates through the heat exchanger

$$(UA)_{eff} = hx_{s,0} + hx_{s,1} \cdot \dot{N}_w + hx_{s,2} \cdot \dot{N}_w^2 + hx_{s,3} \cdot \dot{N}_g + hx_{s,4} \cdot \dot{N}_g^2 \tag{6}$$

where $hx_{s,i}$ are empirical coefficients.

The DC–AC power conditioning efficiency is given by

$$\eta_{PCU} = u_0 + u_1 \cdot P_{el} + u_2 \cdot P_{el}^2 \tag{7}$$

where u_i are empirical coefficients.

Expressions similar to Eqs. (5)–(7) are used to evaluate many of the other terms in the energy balances on a time-step basis.

2.3. Solution procedure

At each time-step of a simulation (typically 1–5 min), the building simulation program invokes the fuel cell micro-cogeneration

[2] Eq. (5) also contains terms that express degradation as a result of operational time and stop–start cycling, but these are omitted here for the sake of clarity.

model and passes it a control signal requesting a given AC power output (P_{AC}). The fuel cell's operating point is established by determining the FCPM's net DC power production (P_{el}) through solution of Eqs. (7) and (3). The electrical efficiency (ϵ_{el}) is calculated with Eq. (5) and the required fuel consumption ($\dot{N}_{fuel}$) determined with Eq. (4). A polynomial expression is used to estimate the enthalpy of each constituent of the fuel (CH_4, C_2H_6, N_2, etc.) as a function of its supply temperature [20]. This along with $\dot{N}_{fuel}$ establishes the first term of Eq. (1) energy balance. Clearly, any errors in the evaluation of Eqs. (3)–(5), and/or (7) or in the ϵ_i or u_i empirical coefficients will lead to errors in the determination of the fuel consumption.

Similar methods are used to establish the other terms of Eq. (1), which is then solved to yield the enthalpy carried out of the control volume by the gas stream ($\dot{H}_{FCPM\text{-}cg}$). The composition of this gas stream is determined by assuming complete reactions between the fuel constituents and the air's O_2,

$$C_xH_y + \left(x + \frac{y}{4}\right) \cdot O_2 \rightarrow x \cdot CO_2 + \frac{y}{2} \cdot H_2O \quad (8)$$

When the flow rates of CO_2 and H_2O determined with Eq. (8) are added to the flow rates of the non-reacting fuel and air constituents, the composition and flow rate ($\dot{N}_g$) of the product gas stream are established. The polynomial function mentioned above is then applied in an iterative manner to establish the temperature ($T_{FCPM\text{-}cg}$) corresponding to the value of $\dot{H}_{FCPM\text{-}cg}$ solved by Eq. (1). Clearly, any errors in the evaluation of any of the above-mentioned equations (and others not mentioned here) or any errors in their empirical coefficients would lead to errors in the estimate of $T_{FCPM\text{-}cg}$.

This temperature is then used in the modelling of the heat exchanger. Firstly, the flow rate of the product gas stream ($\dot{N}_g$) is used to establish $(UA)_{eff}$ using Eq. (6). Eq. (2) is re-arranged and then solved to determine the micro-cogeneration device's useful thermal output (q_{HX}) and the heat exchanger's exiting gas and water temperatures. Once again, any errors in the evaluation of the many terms that lead to $\dot{N}_g$ and $T_{FCPM\text{-}cg}$ will propagate into errors in the prediction of q_{HX}.

3. Model calibration

The previous section outlined some of the model's equations requiring empirical coefficients (5)–(7). These coefficients are the model's inputs. The form of these empirical equations was chosen to facilitate model calibration based upon the testing of coherent fuel cell micro-cogeneration systems. The calibration process essentially involves the design and execution of experiments that isolate the performance of specific aspects of the micro-cogeneration system. Quantities are derived from the measured data and regressions performed to establish the empirical coefficients.

As mentioned in the paper's introduction, such a calibration has been performed for a prototype micro-cogeneration system. The experimental configuration, types of instrumentation employed, operating scenarios examined, uncertainty analysis, and data regression methods are detailed in [13].

Fig. 2 illustrates this effort's calibration of Eq. (5). Seven experiments were performed over a range of P_{el}. For each of these 7 experiments, the value of P_{el} was derived from two voltage measurements and two current measurements (one pair to establish the stack power production less cabling ohmic losses and the other the DC power draw of ancillaries). These derived P_{el} values along with measurements of $\dot{N}_{fuel}$ were used to evaluate Eq. (4) to derive the value of ϵ_{el} for each of the 7 experiments. The value of LHV_{fuel} required by Eq. (4) was derived from the fuel's composition as determined through gas chromatography. The ϵ_{el} values derived from the measurements are plotted along the figure's x-axis. The error bars represent the uncertainty at the 95% confidence level, as determined by propagating instrument bias errors and precision indices using the methods described by [21,22] and as detailed in [13].

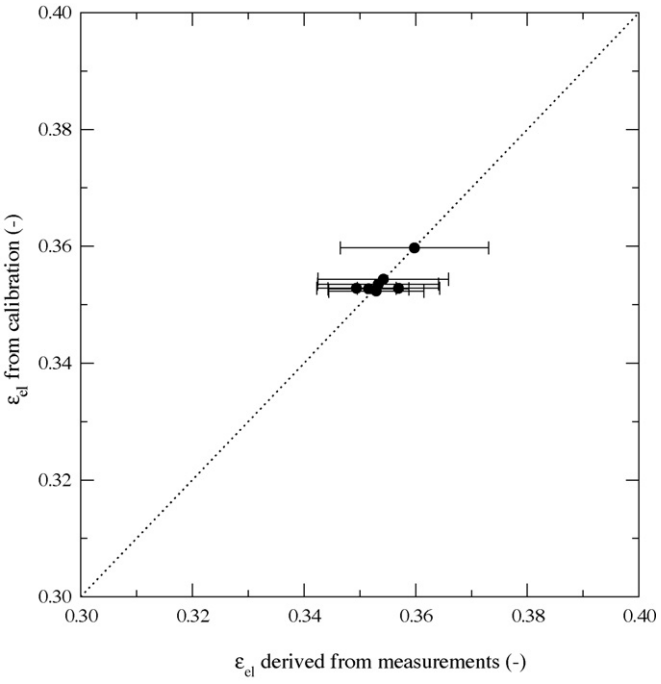

Fig. 2. Eq. 5 versus measurements for calibration experiments.

Table 1
Goodness-of-fit metrics for calibrations of each equation term.

	Average error	Rms error	Max error
ϵ_{el}	0.4%	0.6%	1.2%
$\dot{N}_{air}$	2.3%	2.8%	5.6%
$(UA)_{eff}$	1.9%	2.1%	3.2%
Heat exchanger condensation	11%	12%	21%
η_{PCU}	0.1%	0.2%	0.2%
$q_{FCPM\text{-}to\text{-}dilution}$	3.2%	3.9%	7.7%
$q_{skin\text{-}loss}$	±20% of nominal value		

The experiments resulted in 7 pairs of derived ϵ_{el} and P_{el} values. A non-linear regression of Eq. (5) was performed with these data to yield the calibrated ϵ_i empirical coefficients. The ϵ_{el} subsequently determined with Eq. (5) using these calibrated ϵ_i coefficients are plotted on the y-axis of Fig. 2. Essentially this figure examines the ability of Eq. (5) and the calibrated ϵ_i coefficients to represent the data from which the coefficients were derived. Table 1 presents the average deviation (error) in ϵ_{el} between the calibration and the values derived from the measurements from the 7 experiments. It also presents the root-mean-square (rms) and the maximum errors.

This calibration procedure was repeated for all terms pertinent to this SOFC micro-cogeneration device.[3] Figs. 3 and 4 illustrate the calibration of two of these terms. The former compares the calibrated air supply rate (see the second term of Eq. (1)) against the measured values over the 28 experiments used in this calibration. The latter compares the calibrated value of $q_{FCPM\text{-}to\text{-}dilution}$ (treated as a constant value in the model) against the value derived from measurements for the 7 experiments used in this calibration. The

[3] The model is general in nature and as such includes control volumes and terms not relevant to this particular device.

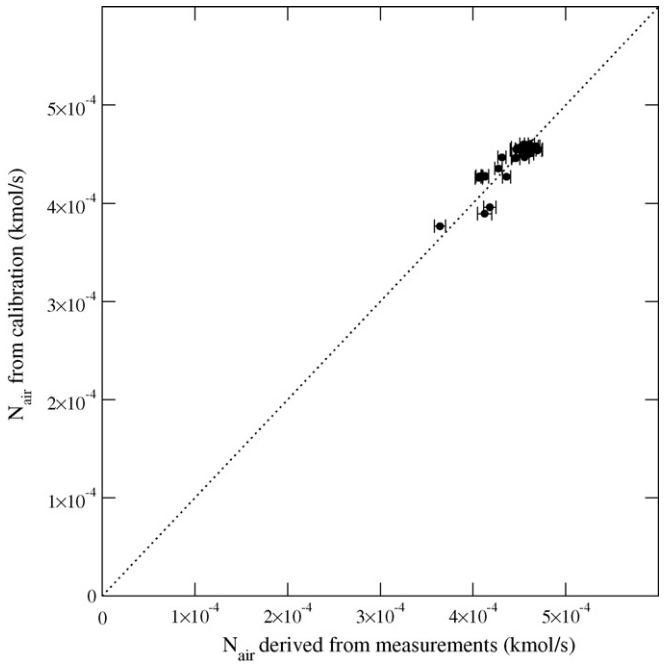

Fig. 3. $\dot{N}_{air}$ calibration versus measurement for calibration experiments.

uncertainty associated with this derived quantity is significant, for reasons explained in [13].

Table 1 presents the goodness-of-fit metrics for these two calibrations, as well as those for most other calibrations pertinent to the SOFC micro-cogeneration device. (The calibration of the FCPM's transient response characteristics are not treated here as they have no bearing upon the subject of the current paper.) An estimated uncertainty rather than goodness-of-fit metrics are presented for the $q_{skin\text{-}loss}$ term of Eq. (1) since it was determined from a single experiment during which infrared images were captured of the micro-cogeneration device's external surfaces. These were used to estimate surface temperatures and classic heat transfer relations

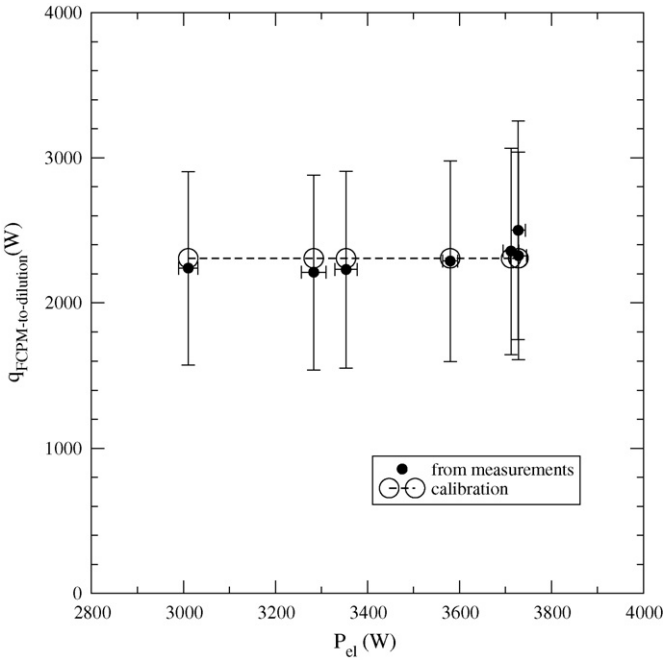

Fig. 4. $q_{FCPM\text{-}to\text{-}dilution}$ calibration versus measurement for calibration experiments.

were used to estimate the free convection and longwave radiation losses. The uncertainty of this calibration of this term was estimated to be 20% of its nominal value of 729 W.

Figs. 2–4 and Table 1 demonstrate that the calibrations of the individual terms of the model accurately represent the calibration data. Worthy of note are the significant uncertainties associated with predicting condensation in the heat exchanger, as well as with the dilution and skin loss heat transfer terms. A more rigorous test of the quality or validity of the calibration as well as the model itself is presented in the next section.

4. Validation approach

4.1. Methodology

The validation of building simulation programs is a complex and challenging field that has existed almost as long as building simulation itself. Extensive efforts have been conducted under the auspices of the International Energy Agency, the American Society of Heating, Refrigerating, and Air-Conditioning Engineers, the European Committee for Standardization (CEN), and others to create methodologies, tests, and standards to verify the accuracy and reliability of building simulation programs. Notable examples include [23–27].

In addition to providing consistent methods for comparing predictions from simulation programs, these initiatives have proven effective at diagnosing errors: inadequacies of simplified mathematical models at representing the thermodynamic processes occurring in reality; mathematical solution inaccuracies; and coding errors (bugs). A pragmatic approach composed of three primary validation constructs to investigate these errors has been widely accepted in the building simulation field [25]:

- Analytical verification.
- Empirical validation.
- Comparative testing.

The second and third methods have been employed to validate the fuel cell micro-cogeneration model. Prior to empirically validating the model, comparative testing was performed to verify the model implementations. The first method, analytical validation, has not been employed due to the complex nature of the devices and the lack of appropriate analytic solutions for the relevant thermodynamic processes.

A general principle applies to all three of these validation constructs. The simpler and more controlled the test case, the easier it is to identify and diagnose sources of error. Realistic cases are suitable for testing the interactions between algorithms, but are less useful for identifying and diagnosing errors. This is because the simultaneous operation of all possible error sources combined with the possibility of offsetting errors means that good or bad agreement cannot be attributed to program validity.

4.2. Comparative testing

The fuel cell micro-cogeneration model has been independently implemented into four simulation platforms. This provided a unique opportunity to apply inter-model comparison testing to diagnose mathematical solution and coding errors. A suite of 50 test cases, each carefully constructed to isolate a specific aspect of the model, was created [28]. Collectively these test cases examine every aspect of the model and exercise each line of its source code implementations.

The comparison of simulation predictions between the four programs revealed numerous solution and coding errors that were

subsequently addressed. As a result, this exercise has verified the implementations of the model: it can be stated with a high-degree of confidence that the source code representations of the model are error free. Consequently in conducting the empirical validation work, any discrepancies between simulation predictions and measurements could be attributed to inadequacies in the mathematical model or to the calibration of its inputs.

5. Empirical validation

Section 4 discussed the technique used to verify the source-code implementations of the model. One of the simulation platforms assessed in this effort, ESP-r [29,30], is applied in this section.

Section 3 summarized how the model has been calibrated to represent the performance of a 2.8 kW_{AC} SOFC micro-cogeneration device using experimental data from the calibration experiments. The current section contrasts simulation predictions and measurements that were taken in a disjunct set of experiments (the validation experiments). Given the above argument, any observed disagreement between simulation predictions and measurements from these 16 validation experiments must be attributable to errors in the mathematical model and/or its calibration and/or in the measurements.

5.1. Time-step comparisons for one experiment

Four boundary conditions fully define the operational state of the micro-cogeneration device:

- The AC power production (see P_{AC} in Eq. (3)).
- The flow rate of water through the heat exchanger (see $\dot{N}_w$ in Eq. (6)).
- The temperature of the cold water at the heat exchanger inlet (see $T_{w\text{-}in}$ in Eq. (2)).
- The temperature of the air supplied to the FCPM (see the $\dot{H}_{air}$ term in Eq. (1)).

These boundary conditions were maintained as constant as possible during each of the 16 validation experiments. Instantaneous measurements of P_{el}, $\dot{N}_{air}$, and $\dot{N}_{fuel}$ were taken every second and the averages over the minute were logged to file. All other measurements were taken every 15 s and the minutely averages logged. Fig. 5 plots the 1-min averages of two of the boundary conditions (P_{AC} and $T_{w\text{-}in}$) over the 10-min duration of one of the validation experiments. The error bars in the figure represent the instrumentation bias errors.

A simulation model was configured to replicate this experiment. The boundary conditions supplied to the simulation model were equivalenced to the 1-min-averaged measurements and a simulation conducted with a 1-min time-step. This boundary condition equivalencing is illustrated in Fig. 5.

By equivalencing the boundary conditions, direct comparisons could then be made between the simulation predictions and the measurements. In keeping with the accepted validation methodology's tenet of simplicity, the FCPM's net DC power production (P_{el}) is the first parameter compared. P_{el} is calculated with Eqs. (3) and (7) using the u_i coefficients and subject to the P_{AC} boundary condition. Therefore, disagreement between the simulation predictions and the measurements would indicate that either or both of these equations were inadequate to represent the performance of the system, that the calibration of the u_i empirical coefficients was deficient, or that there were inaccuracies in the solution of the equations.

The top-left corner of Fig. 6 compares the simulation predictions of P_{el} to the measurements. For presentation clarity the measured

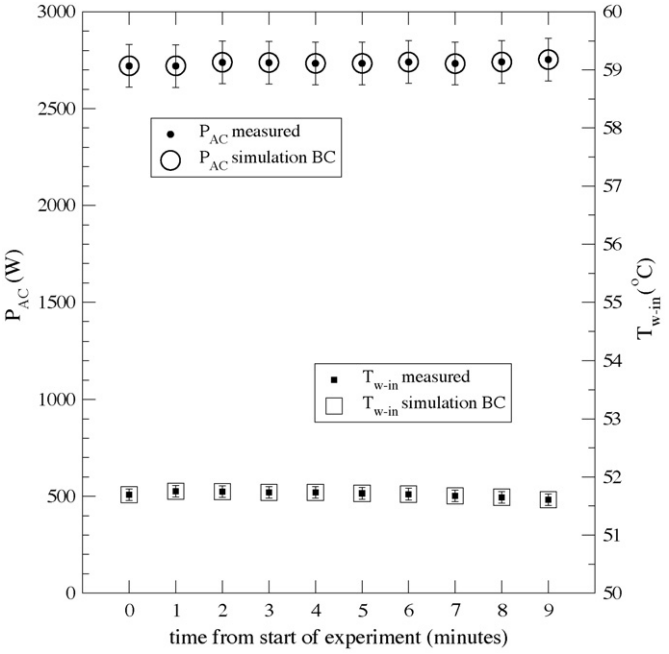

Fig. 5. Equivalencing simulation boundary conditions to replicate measurements.

and simulated quantities have been slightly offset from each other along the *x*-axis. The error bars associated with the measured points represent instrumentation bias errors.

The figure also includes error bars on the simulation predictions. Section 3 described the procedures that were used to calibrate the model using measured data. The model's equations did not perfectly regress these measured data. For example, it was found that the calibrated u_i coefficients could result in up to 0.2% error (see Table 1) in the prediction of η_{PCU} using Eq. (7). Furthermore, uncertainty in the simulation program's prescribed P_{AC} boundary condition would propagate into the prediction of P_{el} using Eq. (3), augmenting the uncertainty in the application of Eq. (7). These uncertainties were propagated using a root-sum-square method [21,22] to estimate the uncertainty associated with the simulation predictions. Thus the error bars associated with the simulation predictions represent the combined uncertainty due to boundary conditions and calibration inaccuracies.

As can be seen from the top-left corner of the figure, the simulation predictions agree with the measurements within the uncertainty associated with the boundary conditions and calibration. Furthermore, the simulation predictions agree with the measurements within the instrumentation bias error at 7 of the 10 1-min intervals. The exception occurs at both the beginning and end of the experiment, where the simulation produces a slightly greater variation in P_{el} from one time-step to the next. (Note the scale of the *y*-axis.) Notwithstanding, the average, rms, and maximum deviation between the simulation predictions and measurements indicates excellent agreement overall (see Table 2). These goodness-of-fit metrics show slightly higher deviation than

Table 2
Goodness-of-fit metrics for time-step simulation predictions for 1 of the 16 validation experiments.

	Average error	Rms error	Max error
P_{el}	0.3%	0.4%	0.8%
$\dot{N}_{fuel}$	2.2%	2.2%	2.9%
$(UA)_{eff}$	1.4%	1.7%	3.5%
q_{HX}	6.7%	6.7%	8.0%

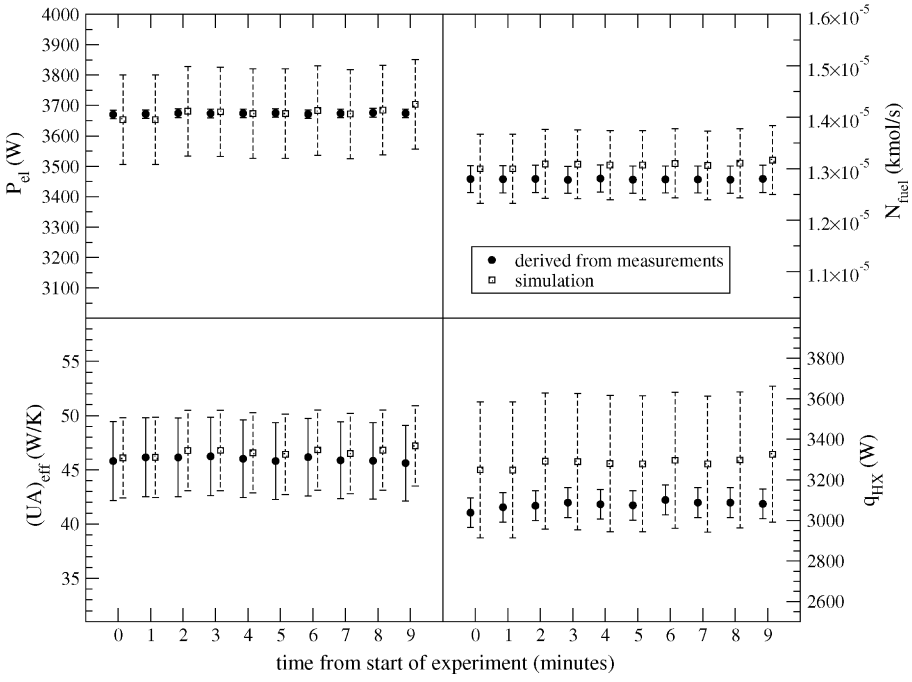

Fig. 6. Time-step comparisons of four key simulation predictions for one experiment.

were observed with the calibration of Eq. (7) (see Table 1) and higher deviation than seen with the P_{AC} boundary condition. However, it can be stated that agreement is very good, with a maximum deviation between simulation and measurement of less than 1%.

The comparisons illustrated in Fig. 6 involve greater interactions between algorithms (i.e. less simplicity) as one moves from left to right and from top to bottom. The top-right corner compares the simulation predictions of the fuel consumption to the measurements. This comparison examines the same aspects of the model as the preceding P_{el} comparison, in addition to Eqs. (4) and (5) and the ϵ_i empirical coefficients (refer to Section 2.3). Once again, the simulation predictions agree with the measurements within the model uncertainty at each of the 1-min intervals. The instrumentation bias error is only 2% of the measured gas flow for this experiment. Notwithstanding, the simulation predictions agree with the measurements within the instrumentation bias error at a number of the 10 1-min intervals and the goodness-of-fit metrics indicate an excellent prediction overall (see Table 2).

The bottom-left corner of Fig. 6 compares the simulation predictions of the heat exchanger's $(UA)_{eff}$ value to the measurements. This examines the validity of the form of Eq. (6) and the $hx_{s,i}$ coefficients. It is worth noting that there was no condensation of water

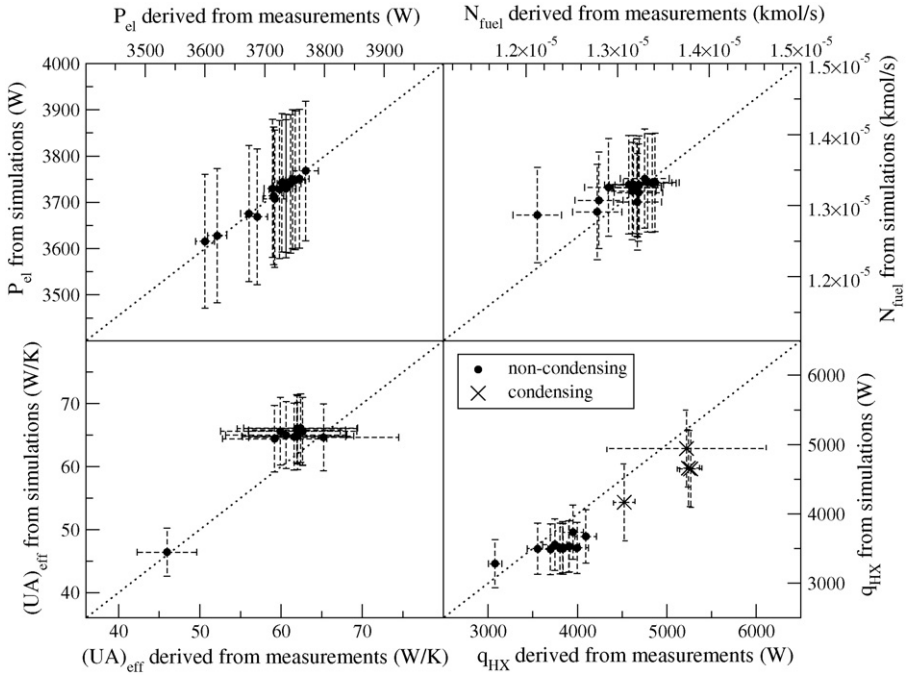

Fig. 7. Time-averaged comparisons of four key simulation predictions for the 16 validation experiments.

Table 3
Goodness-of-fit metrics for simulation predictions for the 16 time-averaged validation experiments.

	Average error	Rms error	Max error
P_{el}	0.2%	0.2%	0.5%
$\dot{N}_{fuel}$	1.2%	1.9%	6.1%
$(UA)_{eff}$	5.4%	6.0%	9.5%
q_{HX}	7.9%	8.4%	12.2%
$\eta_{net\text{-}AC}$	1.2%	1.8%	5.8%
η_{th}	8.5%	8.8%	13%
η_{cogen}	5.3%	5.6%	8.9%

vapour within the heat exchanger during this experiment. In addition, it stresses the aspects of the model that establish $\dot{N}_g$. The simulation predictions agree with the measurements within both the model uncertainty and the instrumentation bias error at each of the 10 1-min intervals. The goodness-of-fit metrics are similar in magnitude to those for the calibration of the $hx_{s,i}$ coefficients (see Table 1).

The bottom-right corner of Fig. 6 compares the simulation predictions of the useful thermal output (q_{HX}) to the measurements. This examines the combined influence of most aspects of the model. Of particular significance is the large uncertainty associated with the $q_{skin\text{-}loss}$ and $q_{FCPM\text{-}to\text{-}dilution}$ terms of Eq. (1) energy balance. Although all measurements lie within the model's uncertainty, as can be seen in the figure, the simulation predictions lie outside the measurement bias uncertainty at all points. However, the goodness-of-fit metrics given in Table 2 are reasonable given the uncertainty associated with the calibration of the two aforementioned heat loss terms: the maximum deviation between simulation predictions and the heat flow derived from measurements is 8%.

5.2. Time-averaged comparisons for 16 validation experiments

The 16 validation experiments varied in duration from 10 min to over 10 h (long experiments were required when condensation formed in the heat exchanger for reasons explained in [13]). The near-constant boundary conditions were time-averaged over each experiment and a simulation model was configured to equivalence these conditions. This resulted in simulation predictions for 16 sets of time-averaged boundary conditions. Averages were then formed from the measured data sets for the same parameters previously examined in the single experiment.

These comparisons are illustrated in Fig. 7. The quantities derived from the measurements are plotted along the x-axis while the simulation predictions are plotted on the y-axis. The diagonals represent the line of perfect agreement. The error bars in the x-direction represent the uncertainty at the 95% confidence level of the time-averaged quantities derived from the measurements. The error bars in the y-direction represent the estimated uncertainties of the model due to uncertainties in boundary conditions and the calibrations. The goodness-of-fit metrics are presented in Table 3.

The top-left corner of Fig. 7 compares the simulation predictions of P_{el} to the measurements. The simulation predictions agree with the measurements within the model uncertainty for all 16 experiments. Furthermore, the model agrees with the measurements within the measurement uncertainly at the 95% confidence level for 14 of the 16 experiments. In one of the outlying experiments the simulation prediction is within 2 W of the measurement uncertainty whereas in the other it is within 1 W.

In general terms, the simulation predictions deviate further from the measurements as complexity increases. Moving from left to right on the graph and from top to bottom involves greater interaction between algorithms and this affords the possibility of uncertainty propagation. Notwithstanding, for 13 of the 16 experiments the simulation predicts the fuel consumption to within the measurement uncertainty at the 95% confidence level (top-right corner). In all experiments the simulation predicts the fuel consumption within the model uncertainty. And for all 16 experiments the simulation predicts the heat exchanger's $(UA)_{eff}$ to within both the model and the measurement uncertainty at the 95% confidence level (bottom-left corner).

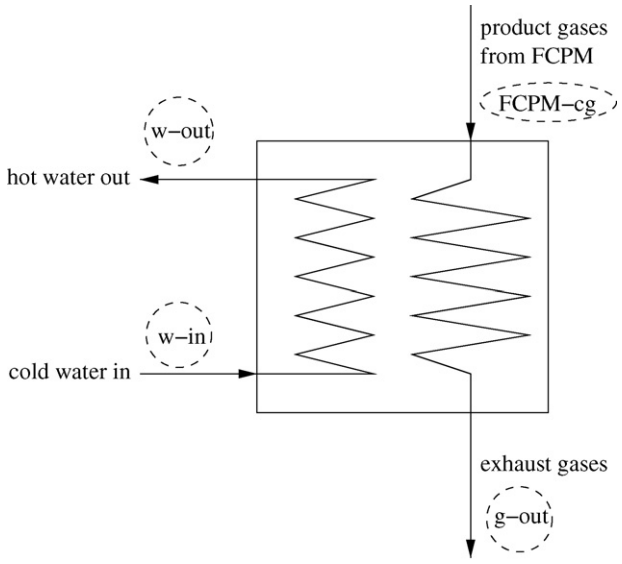

Fig. 8. Exhaust-gas-to-water heat exchanger.

Although the q_{HX} predictions generally agree with the measurements within the model uncertainty (see bottom-right corner of Fig. 7), it appears that there might be a systematic bias. For 15 of the 16 experiments the simulation predicts less heat transfer that the value derived from the measurements and in all but two experiments the simulation predictions lie outside the measurement uncertainty at the 95% confidence level. The average deviation between the simulation predictions and the values derived from measurements is 330 W (~8%) and in one experiment the difference is more than 600 W (12%). The four experiments in which water vapour from the gas stream condensed in the heat exchanger produced the greatest values of q_{HX}. These experiments show some of the greatest deviation between simulation predictions and measurements. As explained earlier there is considerable uncertainty associated with the calibration of this aspect of the model (refer to Table 1).

Further analysis of the measured data was performed to explore this potential systematic bias. This is best explained by examining the schematic representation of the heat exchanger given in Fig. 8. In the previous work [13] the temperatures of all four state points illustrated in this figure (two in the gas stream, two in the liquid water stream) were used to calibrate the heat exchanger's $(UA)_{eff}$ (refer to the sensible term in Eq. (2)). The model assumes that the heat loss from the heat exchanger to the ambient is negligible and that the heat capacity of each fluid stream remains constant through the heat exchanger. Consequently, when no condensation is forming the heat transfer from the hot product gases to the liquid water stream can be calculated with measurements of only the two liquid water state points or only the two gas state points, that is

$$q_{HX} = (\dot{N}\hat{c}_P)_w(T_{water\text{-}out} - T_{water\text{-}in}) = (\dot{N}\hat{c}_P)_g(T_{FCPM\text{-}cg} - T_{g\text{-}out}) \quad (9)$$

where $(\dot{N}\hat{c}_P)_w$ is the product of flow rate (kmol s^{-1}) and heat capacity (J kmol^{-1} K) of the liquid water stream flowing through the heat exchanger; $(\dot{N}\hat{c}_P)_g$ corresponds to these quantities of the gas stream.

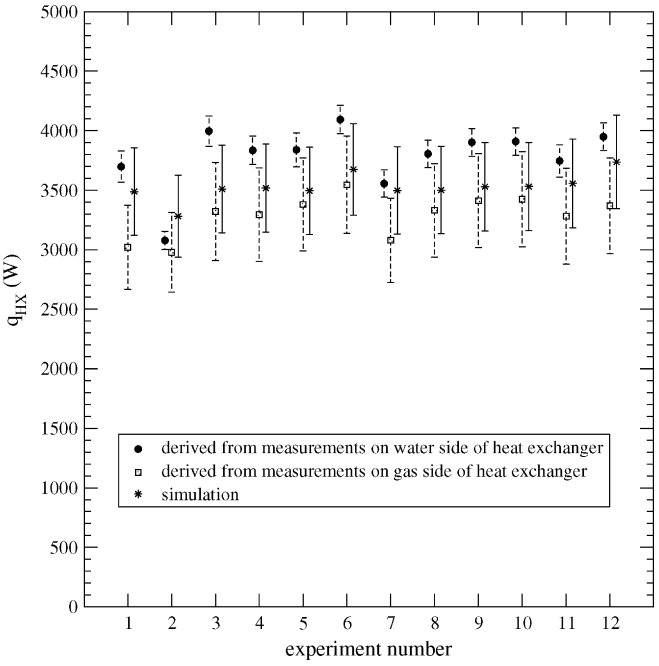

Fig. 9. Contrast of q_{HX} derived from measurements from heat exchanger's liquid water and gas streams.

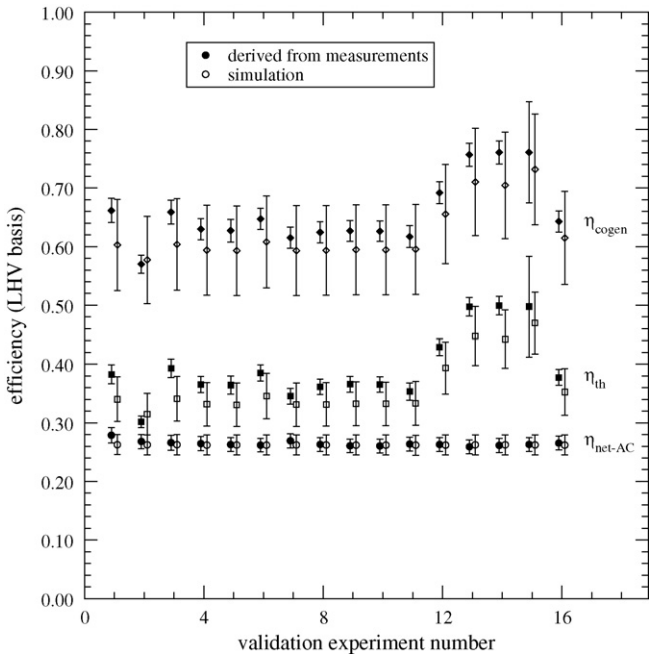

Fig. 10. Time-averaged comparisons of net AC, thermal, and cogeneration efficiencies for the 16 validation experiments.

The q_{HX} values plotted in Fig. 7 are derived from flow rate and temperature measurements taken on the water stream side of the heat exchanger (the left side of Eq. (9). To explore the apparent systematic bias revealed in the bottom-right corner of Fig. 7 the q_{HX} values were derived again, but this time using the flow rate and temperature measurements taken on the gas side of the heat exchanger (the right side of Eq. (9)). The result of this analysis is illustrated in Fig. 9. For each of the 12 experiments during which there was only sensible heat transfer, this figure contrasts the q_{HX} values derived from the two sets of measurements. It also plots the q_{HX} value predicted by simulations with the calibrated model. Once again, for presentation clarity the three sets of data have been slightly offset from each other along the *x*-axis.

As can be seen, in most of the experiments there is a considerable discrepancy between the water-side and gas-side measurements. In all cases, measurements taken on the water side of the heat exchanger resulted in higher values of q_{HX} (by up to 750 W). However, in the majority of experiments the water-side and gas-side measurements agreed within the measurement uncertainty at the 95% confidence level. In 11 of the 12 experiments the simulation predictions lay in between the values derived from the water and gas stream measurements. And in all cases the range of the model uncertainty overlaps with the uncertainty ranges of the measured data.

Based upon these observations it is possible that the error bars in the bottom-right of Fig. 7 underestimate the true experimental uncertainty. These error bars, representing the uncertainty at the 95% confidence interval, were calculated through the propagation of bias errors and measurement precision indices through a root-sum-square method [21,22]. The bias errors were established mainly based upon instrumentation specifications. In some cases instruments were calibrated and in other cases additional bias errors were assigned based upon judgement. As such, the uncertainty bars in the figure represent the errors associated with two calibrated type-T thermocouples (bias errors of 0.1 °C) that measured $T_{w\text{-}in}$ and $T_{w\text{-}out}$ and a water flow meter to measure $\dot{N}_w$ (bias error of ~2%). It is possible that the instrumentation bias errors may have in fact been greater than the manufacturer specifications or instrumentation calibration estimates. Or, that the placement of one or more of the thermocouples may have biased the readings, i.e. it may not have been reading the intended state point.

The final check on the model's validity is made through examining the predictions of three key outputs, the net efficiencies for electrical, useful thermal, and total output from the micro-cogeneration device

$$\eta_{net\text{-}AC} = \frac{P_{AC}}{\dot{N}_{fuel} \cdot LHV_{fuel}} \tag{10}$$

$$\eta_{th} = \frac{q_{HX}}{\dot{N}_{fuel} \cdot LHV_{fuel}} \tag{11}$$

$$\eta_{cogen} = \eta_{net\text{-}AC} + \eta_{th} \tag{12}$$

These three efficiency values would be of prime importance in a simulation-based assessment of the performance of micro-cogeneration systems. As their calculation depends upon the interaction of all aspects of the model, this is perhaps the most challenging comparison of simulation predictions to measurements. The comparison of the simulation predictions of these quantities with the values derived from the measurements are illustrated in Fig. 10 and the goodness-of-fit metrics are presented in Table 3. The thermal efficiencies are derived from the measurements on the liquid water stream using the left side of Eq. (9).

As can be seen, simulation predictions of the electrical efficiency are in better agreement than those for the thermal efficiency. As explained earlier, the error bars representing the uncertainty at the 95% confidence interval possibly underestimate the experimental uncertainty in deriving the thermal efficiency. Notwithstanding, the simulation predictions of the thermal efficiency agree with the measurements within the uncertainly at the 95% confidence level for 5 of the 16 experiments and the measurement and model uncertainties overlap for all experiments. And for 11 of the 16 experiments the simulation predicts the total efficiency within the measurement uncertainty at the 95% confidence level while the measurements are within the model uncertainty in all cases.

6. Conclusions

This paper has examined the validity of a mathematical model—and its calibration to a particular device—for simulating the performance of SOFC micro-cogeneration systems. Pertinent aspects of the mathematical model were described and the methods used to calibrate the model (i.e. establish its inputs) using data gathered through 45 experiments conducted with a prototype 2.8 kW_{AC} SOFC micro-cogeneration device were presented. The methodology used to validate the model, including verifying its implementation into the source code of building simulation programs, was then elaborated. This described how inter-model comparative testing was used to eliminate coding and solution errors.

The paper then described how measured data from 16 experiments (disjunct from the 45 experiments used to calibrate the model) were used to empirically validate the model and its calibration. It showed how simulations were equivalenced with experimental conditions and how measured values and quantities derived from the measurements were compared to simulation predictions. The propagation of measurement uncertainties as well as the propagation of uncertainties in boundary conditions and calibration coefficients into model predictions were considered in these comparisons. These comparisons spanned a range of model parameters, progressing from the simplest case in which only a small subset of the model was exercised, to the complex which involved the concurrent operation and interaction of all aspects of the model.

The paper identified the aspects of the model with the greatest uncertainty, that is the calculation of parasitic thermal losses and the condensation of the exhaust-gas' water vapour within the heat recovery device. The paper explained how this uncertainty could propagate errors into simulation predictions of the useful thermal output. Although this parameter produced the greatest deviations between measurements and simulation predictions, the predictions generally agree with the measurements within the model uncertainty. And in all experiments the range of model uncertainty overlaps with the uncertainty ranges of the measured data.

Good agreement between simulation predictions and measurements was found for other key parameters (e.g. net DC power production, rate of fuel consumption, energy conversion efficiencies) over the range of the 16 experiments. Consequently, it is concluded that the form of the mathematical model can accurately represents the performance of SOFC micro-cogeneration devices and their sub-systems. Furthermore, it has been demonstrated that with the calibration constants determined by [13] the calibrated model can accurately represent the performance of a prototype 2.8 kW_{AC} SOFC micro-cogeneration device. Detailed performance assessments can now be performed using this calibrated model to examine the applicability of this device for supplying building electrical and thermal energy requirements. Additionally, the model can be calibrated to represent the performance of other prototype SOFC micro-cogeneration devices using the techniques elaborated by [13].

Acknowledgements

The work described in this paper was undertaken as part of IEA/ECBCS Annex 42 *Simulation of Building-Integrated Fuel Cell and Other Cogeneration Systems* (http://www.cogen-sim.net). The Annex was an international collaborative research effort and the author gratefully acknowledges the indirect or direct contributions of the other Annex participants. The contributions of Mr. Stephen Oikawa in conducting the experiments and of Ms. Kathleen Lombardi in analyzing the measured data are greatly appreciated. The anonymous reviewers are thanked for their insightful critique and helpful suggestions.

References

[1] I. Knight, V. Ugursal (Eds.), Residential Cogeneration Systems: A Review of the Current Technologies, IEA/ECBCS Annex 42 Report, 2005. ISBN No. 0-662-40482-3.
[2] H. Onovwiona, V. Ugursal, Residential cogeneration systems: review of the current technology, Renewable and Sustainable Energy Reviews 10 (5) (2006) 389–431.
[3] G. Gigliucci, L. Petruzzi, E. Cerelli, A. Garzisi, A.L. Mendola, Demonstration of a residential CHP system based on PEM fuel cells, Journal of Power Sources 131 (1–2) (2004) 62–68.
[4] Y. Hamada, M. Nakamura, H. Kubota, K. Ochifuji, M. Murase, R. Goto, Field performance of a polymer electrolyte fuel cell for a residential energy system, Renewable and Sustainable Energy Reviews 9 (4) (2005) 345–362.
[5] Y. Hamada, R. Goto, M. Nakamura, H. Kubota, K. Ochifuji, Operating results and simulations on a fuel cell for residential energy systems, Energy Conversion and Management 47 (20) (2006) 3562–3571.
[6] W. Münch, H. Frey, M. Edel, A. Kessler, Stationary fuel cells-results of 2 years of operation at EnBW, Journal of Power Sources 155 (1) (2006) 77–82.
[7] M. Radulescu, O. Lottin, M. Feidt, C. Lombard, D. Le Noc, S. Le Doze, Experimental and theoretical analysis of the operation of a natural-gas cogeneration system using a polymer exchange membrane fuel cell, Chemical Engineering Science 61 (2) (2006) 743–752.
[8] M. Davis, A. Fanney, M. LaBarre, K. Henderson, B. Dougherty, Parameters affecting the performance of a residential-scale stationary fuel cell system, Journal of Fuel Cell Science and Technology 4 (2) (2007) 109–115.
[9] M. Davis, Measured performance of three residential fuel cell systems, in: Micro-cogeneration, Proc. 2008, Ottawa, Canada, 2008.
[10] K. Kobayashi, Performance of residential PEMFC cogeneration system in annual actual use, in: Proceedings of the Micro-cogeneration 2008, Ottawa, Canada, 2008.
[11] H. Miura, H. Habara, T. Sawachi, M. Mae, Y. Kuwasawa, Development of evaluation method for micro co-cogeneration in Japan by validation experiment. Part 2. Evaluation of actual performance of PEFC by experiments with occupants' lifestyle simulator, in: Proceedings of the Micro-Cogeneration 2008, Ottawa, Canada, 2008.
[12] H.-S. Chu, F. Tsau, Y.-Y. Yan, K.-L. Hsueh, F.-L. Chen, The development of a small PEMFC combined heat and power system, Journal of Power Sources 176 (2) (2008) 499–514.
[13] I. Beausoleil-Morrison, K. Lombardi, The calibration of a model for simulating the thermal and electrical performance of a 2.8 kwAC solid-oxide fuel-cell micro-cogeneration device, Journal of Power Sources 186 (1) (2009) 67–79.
[14] G. Mulder, P. Coenen, A. Martens, J. Spaepen, The development of a 6kw fuel cell generator based on alkaline fuel cell technology, International Journal of Hydrogen Energy 33 (12) (2008) 3220–3224.
[15] U.C. Colpier, D. Cornland, The economics of the combined cycle gas turbine—an experience curve analysis, Energy Policy 30 (4) (2002) 309–316.
[16] T. DeMoss, Theyŕe he-e-re (almost): the 60% efficient combined cycle, Power Engineering 100 (7) (1996) 17–21.
[17] I. Beausoleil-Morrison, A. Schatz, F. Maréchal, A model for simulating the thermal and electrical production of small-scale solid-oxide fuel cell cogeneration systems within building simulation programs, Journal of HVAC&R Research Special Issue 12 (3a) (2006) 641–667.
[18] N. Kelly, I. Beausoleil-Morrison (Eds.), Specifications for Modelling Fuel Cell and Combustion-Based Residential Cogeneration Devices within Whole-Building Simulation Programs, IEA/ECBCS Annex 42 Report, 2007. ISBN No. 978-0-662-47116-5.
[19] I. Beausoleil-Morrison (Ed.), Experimental Investigations of Residential Cogeneration Devices and Model Calibration, IEA/ECBCS Annex 42 Report, 2007. ISBN No. 978-0-662-47523-1.
[20] P. Linstrom, W. Mallard (Eds.), NIST Chemistry WebBook, NIST Standard Reference Database Number 69, National Institute of Standards and Technology, Gaithersburg, USA.
[21] R. Moffat, Describing the uncertainties in experimental results, Experimental Thermal and Fluid Science 1 (1988) 3–17.
[22] R. Abernethy, R. Benedict, R. Dowdell, ASME measurement uncertainty, Journal of Fluids Engineering 107 (1985) 161–164.
[23] S. Jensen (Ed.), Validation of Building Energy Simulation Programs, Part I and II, PASSYS Subgroup Model Validation and Development, 1993. eUR 15115 EN.
[24] K. Lomas, H. Eppel, C. Martin, D. Bloomfield, Empirical Validation of Thermal Building Simulation Programs Using Test Room Data, vol. 1: Final Report, IEA ECBCS Annex 21 and IEA SHC Task 12, 1994.
[25] R. Judkoff, J. Neymark, International Energy Agency Building Energy Simulation Test (BESTEST) and Diagnostic Method, IEA/ECBCS Annex 21 Subtask C and IEA/SHC Task 12 Subtask B Report, 1995.
[26] CEN, prEN ISO 13791: Thermal Performance of Buildings Calculation of Internal Temperatures of a Room in Summer Without Mechanical Cooling—General Criteria and Validation Procedures, ISO/FDIS 13791:2004, Brussels, Belgium, 2004.
[27] ANSI/ASHRAE, Standard Method of Test for the Evaluation of Building Energy Analysis Computer Programs, Standard 140-2007, Atlanta, USA, 2007.

[28] I. Beausoleil-Morrison, B. Griffith, T. Vesanen, A. Weber, A demonstration of the effectiveness of inter-program comparative testing for diagnosing and repairing solution and coding errors in building simulation programs, Journal of Building Performance Simulation 2 (1) (2009) 63–73.
[29] ESRU, The ESP-r system for building energy simulations: user guide version 10 series, Tech. Rep. U05/1, University of Strathclyde, Glasgow, UK, 2005.
[30] J. Clarke, Energy Simulation in Building Design, 2nd ed., Butterworth-Heinemann, Oxford, UK, 2001.